STRUCTURAL BIOLOGY COMMUNICATIONS

ISSN 2053-230X

Solution NMR structures of oxidized and reduced *Ehrlichia chaffeensis* thioredoxin: NMR-invisible structure owing to backbone dynamics

Garry W. Buchko,[a,b,c]* Stephen N. Hewitt,[a,d] Wesley C. Van Voorhis[a,d,e,f] and Peter J. Myler[a,e,g,h]

[a]Seattle Structural Genomics Center for Infectious Disease, USA, [b]Earth and Biological Sciences Directorate, Pacific Northwest National Laboratory, Richland, Washington, USA, [c]School of Molecular Biosciences, Washington State University, Pullman, Washington, USA, [d]Department of Medicine, Division of Allergy and Infectious Disease, University of Washington, Seattle, Washington, USA, [e]Department of Global Health, University of Washington, Seattle, Washington, USA, [f]Department of Microbiology, University of Washington, Seattle, Washington, USA, [g]Center for Infectious Disease Research, Seattle, Washington, USA, and [h]Department of Biomedical Informatics and Health Education, University of Washington, Seattle, Washington, USA. *Correspondence e-mail: garry.buchko@pnnl.gov

Received 9 October 2017
Accepted 16 December 2017

Edited by G. G. Privé, University of Toronto, Canada

Keywords: human monocytic ehrlichiosis; infectious diseases; thioredoxin; reactive oxygen species; structural biology; molecular dynamics; *Ehrlichia chaffeensis*; NMR.

PDB references: oxidized *Ec*-Trx, 6ali; reduced *Ec*-Trx, 6amr

Supporting information: this article has supporting information at journals.iucr.org/f

Thioredoxins are small ubiquitous proteins that participate in a diverse variety of redox reactions *via* the reversible oxidation of two cysteine thiol groups in a structurally conserved active site. Here, the NMR solution structures of a reduced and oxidized thioredoxin from *Ehrlichia chaffeensis* (*Ec*-Trx, ECH_0218), the etiological agent responsible for human monocytic ehrlichiosis, are described. The overall topology of the calculated structures is similar in both redox states and is similar to those of other thioredoxins: a five-stranded, mixed β-sheet (β1–β3–β2–β4–β5) surrounded by four α-helices. Unlike other thioredoxins studied by NMR in both redox states, the ^{1}H–^{15}N HSQC spectrum of reduced *Ec*-Trx was missing eight additional amide cross peaks relative to the spectrum of oxidized *Ec*-Trx. These missing amides correspond to residues Cys35–Glu39 in the active-site-containing helix (α2) and Ser72–Ile75 in a loop near the active site, and suggest a change in backbone dynamics on the millisecond-to-microsecond timescale associated with the breakage of an intramolecular Cys32–Cys35 disulfide bond in a thioredoxin. A consequence of the missing amide resonances is the absence of observable or unambiguous NOEs to provide the distance restraints necessary to define the N-terminal end of the α-helix containing the CPGC active site in the reduced state. This region adopts a well defined α-helical structure in other reported reduced thioredoxin structures, is mostly helical in oxidized *Ec*-Trx and CD studies of *Ec*-Trx in both redox states suggests there is no significant difference in the secondary structure of the protein. The NMR solution structure of reduced *Ec*-Trx illustrates that the absence of canonical structure in a region of a protein may be owing to unfavorable dynamics prohibiting NOE observations or unambiguous NOE assignments.

1. Introduction

Thioredoxins are small proteins of approximately 100 residues that are found in organisms ranging from archaea to mammals and participate in a diverse variety of redox reactions *via* the reversible oxidation of two cysteine thiol groups to a disulfide (Holmgren, 1985, 1995). In the reducing environment inside the cell the primary function of Trxs is to prevent the formation of unwanted disulfide bonds (Collet & Messens, 2010), especially in metabolically essential enzymes such as ribonucleotide reductase (Laurent *et al.*, 1964). Thioredoxins protect proteins from oxidative aggregation and inactivation (Holmgren, 1985, 1995), are a critical component of cellular antioxidant defense strategies against reactive oxygen and

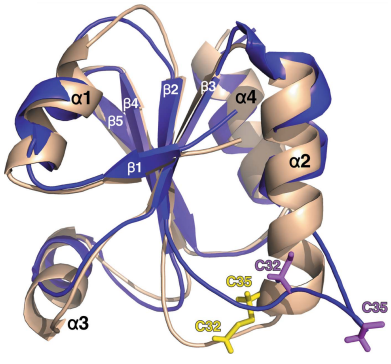

nitrogen species (Lu & Holmgren, 2014), play a role in regulation of apoptosis (Ravi *et al.*, 2005), act as growth factors and modulate inflammatory responses (Powis *et al.*, 2000). Once oxidized, Trxs are reduced by thioredoxin reductase *via* an NADPH-dependent reaction to reactivate the Trxs (Mustacich & Powis, 2000).

Human monocytic ehrlichiosis is an important emerging infectious disease in the United States (Paddock & Childs, 2003). The pathogen responsible, *Ehrlichia chaffeensis*, is an obligate intracelluar bacterium in the Anaplasmataceae family (Rikihisa, 2010) that is transmitted between mammals by the blood-sucking arthropod *Amblyomma americanum* (also known as the lone star tick; Ewing *et al.*, 1995). Clinical symptoms of human monocytic ehrlichiosis include headache, fever, myalgia, anorexia and chills. While the severity of the disease may be limited to asymptomatic seroconversion, because *E. chaffeensis* replicates inside mammalian monocyte and macrophage cells, infection may lead to leukopenia and life-threatening complications such as kidney or respiratory failure. Consequently, human monocytic ehrlichiosis may represent the most prevalent life-threatening tick-borne infection in the United States (Olano & Walker, 2002). No vaccines against human monocytic ehrlichiosis exist and the choice of antibiotics available to treat infection is currently limited to doxycycline and rifampin, with the effectiveness of these treatments reduced if initiation of treatment is delayed. Since reactive oxygen species are abundantly produced by host monocytes and macrophages, it is expected that a robust Trx system is vital for intracellular survival of *E. chaffeensis* (Lu & Holmgren, 2014), and thus Trx inhibition may represent an intervention strategy for human monocytic ehrlichiosis. The 107-residue protein ECH_0218 (*Ec*-Trx) has been identified as a Trx in *E. chaffeensis*. To assist structure-based drug design (Staker *et al.*, 2015) targeting *Ec*-Trx and to better understand cellular redox mechanisms, we describe the NMR solution structure and backbone dynamic features of *Ec*-Trx in the oxidized and reduced states.

2. Materials and methods

2.1. Cloning, expression and purification

The Ec-*Trx* gene (ECH_0218, YP_507041.1) was PCR-amplified using the genomic DNA of *E. chaffeensis* (strain Arkansas) and the oligonucleotide primers 5′-**GGGT CCTGGTTCGA**TGATTGAGCAAATTGGAGACAGTG-3′ (forward) and 5′-**CTTGTTCGTGCTGTTTATTA**GTTTATA TTGTTATTTATTTCACTAATTAT-3′ (reverse) (Invitrogen, Carlsbad, California, USA) containing LIC primers (bold). To enable protein purification by metal-chelation chromatography (Choi *et al.*, 2011), the amplified Ec-*Trx* gene was inserted into the NruI/PmeI-digested expression vector AVA0421 by ligation-independent cloning such that the N-terminus of the expressed gene product contained a 21-residue extension: MAHHHHHHMGTLEAQTGPGS–. A heat-shock method was then used to transform the recombinant plasmid into *Escherichia coli* BL21(DE3)-R3-pRARE2 cells (a gift from SGC Toronto, Ontario, Canada). 750 ml of minimal medium (Miller) containing $^{15}NH_4Cl$ (1 mg ml^{-1}), D-[$^{13}C_6$]-glucose (2.0 mg ml^{-1}), NaCl (50 µg ml^{-1}), $MgSO_4$ (120 µg ml^{-1}), $CaCl_2$ (11 µg ml^{-1}), Fe_2Cl_3 (10 ng ml^{-1}) chloramphenicol (35 µg ml^{-1}) and ampicillin (100 µg ml^{-1}) was used to obtain uniformly ^{15}N,^{13}C-labeled *Ec*-Trx. The transformed cells were grown at 37°C to an OD_{600} of ∼0.8, transferred to a 25°C incubator and protein expression was induced with isopropyl β-D-1-thiogalactopyranoside (0.026 µg ml^{-1}). Approximately 4 h later the cell culture was harvested by mild centrifugation and frozen (−80°C). *Ec*-Trx was purified from the thawed pellet using a conventional two-step protocol: metal-chelate affinity chromatography on a 20 ml Ni-Agarose 6 FastFlow column (GE Healthcare, Piscataway, New Jersey, USA) followed by gel-filtration chromatography on a Superdex 75 HiLoad 26/60 column (GE Healthcare). The only difference between the protocols used to prepare oxidized and reduced *Ec*-Trx was the addition of 1 m*M* dithiothreitol (DTT) to the gel-filtration buffer (100 m*M* NaCl, 20 m*M* Tris pH 7.1) to obtain the reduced state.

2.2. Circular dichroism spectroscopy

An Aviv Model 410 spectropolarimeter (Lakewood, New Jersey, USA) was used to collect circular dichroism data from a 400 µl sample of ∼0.07 m*M* *Ec*-Trx in a quartz cell of 0.1 cm path length. A steady-state wavelength spectrum was first collected for oxidized *Ec*-Trx at 20°C in buffer containing no DTT (100 m*M* NaCl, 20 m*M* Tris pH 7.0). The same sample was then made 1.0 m*M* in DTT and the spectrum of reduced *Ec*-Trx was recorded 1 h later. Thermal denaturation curves were obtained for *Ec*-Trx in both states by recording the ellipticity at 220 nm in 2.0°C intervals from 10 to 90°C. The reported steady-state wavelength spectrum is the average of two consecutive scans, collected with a bandwidth of 1.0 nm and a time constant of 1.0 s, processed by subtracting a blank spectrum from the protein spectrum and automatic line smoothing using the *AVIV* software.

2.3. Nuclear magnetic resonance spectroscopy

All NMR data were collected from double-labeled (^{13}C,^{15}N) samples of *Ec*-Trx (∼1.0 m*M*) using Agilent spectrometers operating at ^1H resonance field strengths of approximately 600, 750 or 800 MHz. All spectrometers were equipped with an HCN probe, pulse-field gradients and *Varian Biopack* software. Because the ^1H–^{15}N HSQC spectrum of reduced *Ec*-Trx contained the best amide cross peak line shape and chemical shift dispersion at 20°C, NMR data for both *Ec*-Trx redox states were collected at this temperature. For reduced *Ec*-Trx, the ^1H, ^{13}C and ^{15}N chemical shifts of the backbone and side-chain resonances were assigned from analysis of two-dimensional ^1H–^{15}N HSQC, ^1H–^{13}C HSQC, HBCBCGCDHD and HBCBCGCDCHE spectra and three-dimensional HNCACB, CBCA(CO)NH, HCC-TOCSY-NNH, CC-TOCSY-NNH and HNCO spectra. Because the ^1H–^{15}N HSQC spectrum of oxidized *Ec*-Trx was similar to the ^1H–^{15}N HSQC spectrum of reduced *Ec*-Trx, fewer NMR experiments were

required to assign the ^{1}H, ^{13}C and ^{15}N chemical shifts for oxidized *Ec*-Trx: two-dimensional ^{1}H-^{15}N HSQC and ^{1}H–^{13}C HSQC spectra and three-dimensional CC-TOCSY-NNH and HNCO spectra. For samples in both redox states, three-dimensional ^{15}N-edited NOESY-HSQC and ^{13}C-edited NOESY-HSQC (aliphatic and aromatic) spectra, collected with a mixing time of 85 ms, were analyzed to obtain the side-chain ^{1}H assignments and the NOE-based distance restraints required for the structure calculations. Slowly exchanging amides were identified by lyophilizing the double-labeled (^{13}C,^{15}N) samples, re-dissolving them in 99.8% D_2O and immediately collecting a ^{1}H–^{15}N HSQC spectrum (∼10 min later). Steady-state {^{1}H}–^{15}N heteronuclear NOE values (NOE = I_{sat}/I_{unsat}) were measured (20°C, 600 MHz ^{1}H resonance field strength) in triplicate by taking the ratio of ^{1}H–^{15}N HSQC cross-peak heights in spectra recorded in the presence (I_{sat}) and absence (I_{unsat}) of 3.0 s of proton presaturation prior to the ^{15}N excitation pulse (Farrow *et al.*, 1994). *Felix*2007 (MSI, San Diego, California, USA) and *Sparky* (v.3.115) were used to process and analyze, respectively, all of the NMR data. The ^{1}H, ^{13}C and ^{15}N chemical shifts were referenced using indirect methods (DSS = 0 p.p.m.) and deposited in the Biological Magnetic Resonance Bank database (http://www.bmrb.wisc.edu) under accession numbers BMRB-19452 and BRMB-19938 for reduced and oxidized *Ec*-Trx, respectively.

2.4. Structure calculations

Using the ^{1}H, ^{13}C and ^{15}N chemical shift assignments and peak-picked NOESY data as initial experimental inputs, solution structures for *Ec*-Trx in the oxidized and reduced states were determined with the programs *CYANA* (v.2.1) and *CNS* (v.1.1) following previously described protocols (Buchko *et al.*, 2015; Buchko, Hewitt *et al.*, 2013). On the basis of preliminary structure calculations and chemical shift trends, six restraints between the side-chain S atoms of Cys32 and Cys35 (2.0–2.1, 3.0–3.1 and 3.0–3.1 Å for the S^{γ}—S^{γ}, S^{γ}—C^{β} and C^{β}—S^{γ} distances, respectively) were introduced into the structure calculations to fix this disulfide bond in oxidized *Ec*-Trx (Sagaram *et al.*, 2013). It was not possible to assign the side-chain atoms (^{13}C and ^{1}H) of the third conserved proline, Pro76, in *Ec*-Trx and unambiguously identify the conformational state of Pro76 based on the intra-residue NOE pattern between proline side-chain protons. In all reported Trx structures the third conserved proline residue is exclusively observed in the *cis* conformation (Collet & Messens, 2010), and therefore, this assumption was made in our structure calculations and Pro76 was constrained to the *cis* conformation in the structure calculations. The final ensemble of 20 *CYANA*-derived structures was refined with explicit waters with *CNS* (v.1.1) using the PARAM19 force field and force constants of 500, 500 and 1000 kcal for the NOE, hydrogen-bond and dihedral restraints, respectively. For these water refinement calculations, the upper boundary of the *CYANA* distance restraints was increased by 10% for reduced *Ec*-Trx and 5% for oxidized *Ec*-Trx, with the lower boundary set to the van der Waals limit for both. Structure quality was assessed with the online *Protein Structure Validation Suite* (*PSVS* v.1.5; Bhattacharya *et al.*, 2007) and these values are included in the summary of structure statistics in Table 1. Atomic coordinates for the final ensemble of 20 structures for reduced and oxidized *Ec*-Trx were deposited in the Research Collaboratory for Structural Bioinformatics (RCSB) Protein Data Bank (PDB) under PDB codes 6amr and 6ali, respectively. Note that while the protein sequence in the BMRB and PDB is numbered continuously, Met1–Asn107, here the first native residue (Met22 in the BMRB and PDB sequence) is numbered Met1.

Table 1
Summary of the structural statistics for *Ec*-Trx in the reduced and oxidized states.

All statistics are for the 20-structure ensemble deposited in the Protein Data Bank.

Ec-Trx	Reduced	Oxidized
PDB code	6amr	6ali
BMRB code	BRMB-19452	BRMB-19938
Restraints for structure calculations		
Total NOEs	1454	1724
Intraresidue NOEs	378	487
Sequential (i, i + 1) NOEs	407	486
Medium-range (i, i + j; 1 < j ≤ 4) NOEs	294	332
Long-range (i, i + j; j > 4) NOEs	375	419
φ angles	75	77
ψ angles	75	77
Hydrogen bonds	32	44
Disulfide bonds	—	1
Structure calculations		
No. of structures calculated	100	100
No of structures used in ensemble	20	20
Structures with restraint violations		
Distance restraint violations > 0.05 Å	0	0
Dihedral restraint violations > 6°	0	1
R.m.s.d. to mean (Å) (residues Met1–Asn107)		
Backbone N—C^{α}—C═O atoms	1.54 ± 0.24	0.82 ± 0.18
All heavy atoms	2.09 ± 0.24	1.31 ± 0.21
R.m.s.d. to mean (Å) (*PSVS* ordered residues)		
Backbone N—C^{α}—C═O atoms	0.75 ± 0.15	0.71 ± 0.16
All heavy atoms	1.20 ± 0.17	1.07 ± 0.14
Ramachandran plot summary†		
Most favored regions (%)	95.8	96.7
Additionally allowed regions (%)	3.7	3.1
Generously favored regions (%)	0.4	0.2
Disallowed (%)	0	0
Global quality scores (Met1–Asn107)		
PROCHECK *Z*-score (raw) (all)	−2.54 (−0.43)	−1.06 (−0.18)
PROCHECK *Z*-score (raw) (φ, ψ)	−0.97 (−0.30)	−0.24 (−0.14)
MolProbity clash score	−3.99 (32.14)	−3.44 (28.91)

† Calculated using *MolProbity* (Chen *et al.*, 2010) with residues Met1–Ile107.

3. Results and discussion

3.1. Solution structure of reduced and oxidized *Ec*-Trx

Fig. 1 shows a superposition of the ordered regions of the ensemble structure closest to the average for reduced (PDB entry 6amr, purple) and oxidized (PDB entry 6ali, wheat) *Ec*-Trx generated using the program *SuperPose* (Maiti *et al.*, 2004). As observed in both NMR and X-ray crystallographic structures of other oxidized and reduced Trxs (Holmgren,

1985, 1995; Jeng *et al.*, 1994; Amorim *et al.*, 2007; Olson *et al.*, 2013; Peterson *et al.*, 2005; Qin *et al.*, 1994; Stefanková *et al.*, 2005; Collet & Messens, 2010), *Ec*-Trx is composed of a five-stranded, twisted, mixed β-sheet ($\uparrow\uparrow\uparrow\downarrow\uparrow$; $\beta1$–$\beta3$–$\beta2$–$\beta4$–$\beta5$) surrounded by four α-helices. Helices $\alpha1$ and $\alpha3$ are located on one face of the β-sheet and helices $\alpha2$ and $\alpha4$ on the opposite face, with $\alpha3$ approximately perpendicular to $\alpha2$ and $\alpha4$. The catalytic CGPC motif, Cys32–Cys35, is located at the N-terminal end of $\alpha2$, exposed to the surface of the protein. The reduced and oxidized structures are generally similar, with a backbone r.m.s.d. of 2.0 Å between ordered regions. The most significant difference between the two structures obtained from the available NMR data is the length of $\alpha2$, which extends between residues Pro34 and Tyr49 in the oxidized state but only between residues Gln41 and Glu51 in the reduced state (Fig. 1*b*). This difference appears to contrast with the crystal and NMR structures of other Trxs in both redox states, where no such dramatic change in $\alpha2$ was observed (Holmgren, 1985, 1995; Jeng *et al.*, 1994; Olson *et al.*, 2013; Peterson *et al.*, 2005; Qin *et al.*, 1994; Stefanková *et al.*, 2005; Collet & Messens, 2010). For example, in the NMR solution structures of human Trx and *Mycobacterium tuberculosis* TrxC in both redox states, the backbones of the region containing the active-site cysteine residues form part of an α-helix and superimpose well (Qin *et al.*, 1994; Olson *et al.*, 2013), with only the side-chain S–S distance increasing (1–1.5 Å) on going from the oxidized to the reduced state. Was the difference observed between the two NMR-based structures of *Ec*-Trx real or a consequence of the available NMR data for the structure calculations?

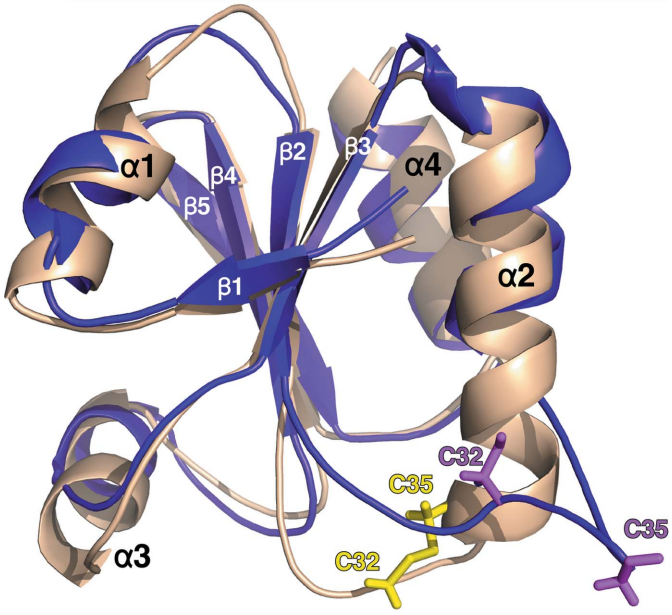

(*a*)

```
          β1       α1                 β2                 α2
re MIEQIGDSEF DNKVTSCNDN ILILVDFWAP WCGPCRSLEP  40
ox MIEQIGDSEF DNKVTSCNDN ILILVDFWAP WCGPCRSLEP  40

                  β3                 α3          β4
re QLEKLAQQYT ENVKIYKIDI DDNQDVATQY GVSAIPTILM  80
ox QLEKLAQQYT ENVKIYKIDI DDNQDVATQY GVSAIPTILM  80

          β5       α4
re FKNGKKLSQV IGADISKIIS EINNNIN                107
ox FKNGKKLSQV IGADISKIIS EINNNIN                107
```

(*b*)

Figure 1
(*a*) Superposition of cartoon representations of the structures of oxidized (PDB entry 6ali, wheat) and reduced (PDB entry 6amr, purple) *Ec*-Trx closest to the average structure in the calculation ensembles. The 21-residue N-terminal tag has been removed for clarity, with the side chains of the active-site cysteine residues, Cys32 and Cys35, colored yellow (oxidized) and magenta (reduced). (*b*) The primary structure of *Ec*-Trx with the *STRIDE* elements of secondary structure identified in the reduced (*re*) and oxidized (*ox*) states (α-helices, red; β-strands, blue). Residues lacking an assigned amide cross peak are identified by hollow letters.

3.2. Chemical shift verification of cysteine oxidation states

Foremost in assessing the NMR structural differences in $\alpha2$ is to ascertain the oxidation state and disulfide-bond pairings of the cysteine residues under both conditions used in the structure calculations. The two cysteine residues in the active-site CGPC motif are conserved in all Trxs and are essential for catalytic activity (Collet & Messens, 2010). In addition to the two cysteine residues, Cys32 and Cys35, in the CGPC motif of *Ec*-Trx, a third cysteine, Cys17, is also present in the primary amino-acid sequence of *Ec*-Trx. Because the chemical shift of the cysteine C^{β} atom is sensitive to the redox state of the cysteine S^{γ} atom, it can be used to infer the redox states of cysteine residues in a protein (Sharma & Rajarathnam, 2000). Generally, the cysteine $^{13}C^{\beta}$ chemical shift in the reduced state is <32 p.p.m. and increases to >35 p.p.m. in the oxidized state. The Cys17 $^{13}C^{\beta}$ chemical shift changes little in the presence (27.8 p.p.m.) and absence (27.9 p.p.m.) of the reductant DTT, unambiguously verifying that Cys17 in *Ec*-Trx is a free thiol under both conditions. While this is expected in the presence of DTT, in the absence of DTT this observation indicates that Cys17 is not forming intermolecular or intramolecular disulfide bonds. On the other hand, out of the two remaining cysteine residues, only the $^{13}C^{\beta}$ chemical shift for Cys35 in the absence of DTT could be assigned because it was the only other cysteine amide that was detected in the ^{1}H–^{15}N HSQC spectrum under both conditions (Fig. 1*b*). At 35.7 p.p.m., the Cys35 $^{13}C^{\beta}$ chemical shift is consistent with the formation of an oxidized cysteine participating in a disulfide bond. The possibility of Cys35–Cys35 intermolecular disulfide-bond formation is excluded as both oxidized and reduced *Ec*-Trx eluted from a size-exclusion column with a retention time characteristic of a monomer (data not shown). Because the $^{13}C^{\beta}$ chemical shift for Cys17 is characteristic of a reduced cysteine, by elimination Cys35 must be forming a disulfide bond with Cys32. As described in §2.4, these chemical shift trends, along with proximity in preliminary structure calculations, were used to justify the introduction of six restraints between the side-chain S atoms of Cys32 and Cys35 in the structure calculations.

3.3. Data and structure quality

The ^{1}H–^{15}N HSQC spectrum for reduced *Ec*-Trx shown in Fig. 2(*a*) contains amide cross peaks with good chemical shift dispersion in both the ^{1}H and ^{15}N dimensions characteristic of

a structured protein (Yee *et al.*, 2002). In the absence of the reductant DTT the ^{1}H–^{15}N HSQC spectrum for oxidized *Ec*-Trx, shown in Fig. 2(*b*), was generally similar to the spectrum for reduced *Ec*-Trx except for the appearance of eight amide cross peaks (circled in orange in Fig. 2*b*) and more uniform amide cross-peak intensities. Cross peaks were also missing for ten backbone amides in *Ec*-Trx in both redox states. Missing amide resonances in ^{1}H–^{15}N HSQC spectra of Trxs appear to be uncommon in either redox state. One missing amide resonance at the second cysteine in the CGPC motif was reported in the ^{1}H–^{15}N HSQC spectrum of reduced *Saccharomyces cerevisiae* Trx2 (Amorim *et al.*, 2007). Instead of disappearing amide resonances in ^{1}H–^{15}N HSQC spectra, a subset of amide cross peaks are usually observed to shift markedly in ^{1}H–^{15}N HSQC spectra of reduced and oxidized Trxs, as shown for human (Qin *et al.*, 1994), *E. coli* (Jeng *et al.*, 1994), *Arabidopsis thaliana* (Peterson *et al.*, 2005) and *M. tuberculosis* (Olson *et al.*, 2013) Trxs. In these examples, the overall backbone of solution structures for α2 determined in both redox states was similar except for slight differences in the region of the active site corresponding to amides with the observed chemical shift perturbations. Missing amide resonances have been observed at a dimer interface (Buchko *et al.*, 2017); however, size exclusion column chromatography showed that *Ec*-Trx was monomeric in both redox states (§3.2) as is common for Trxs (Eklund *et al.*, 1991). Missing or non-uniform amide resonances may also be indicative of transient association (Buchko, Lin *et al.*, 2013); however, no significant changes in the ^{1}H–^{15}N HSQC spectra were observed following a tenfold dilution of the NMR samples used in our studies (data not shown). Instead, the missing amide cross peaks in the ^{1}H–^{15}N HSQC spectrum of reduced *Ec*-Trx observed here are likely to signify that this region of the protein is undergoing chemical exchange on an intermediate timescale (milliseconds to microseconds; Buchko *et al.*, 1999; Ådén *et al.*, 2011). For example, amide resonances in ^{1}H–^{15}N HSQC spectra have been observed to disappear in peroxiredoxins as a function of the redox state of a single pair of intramolecular cysteine residues, with the disappearance attributed to substantial changes in backbone dynamics (Ådén *et al.*, 2011; Buchko *et al.*, 2016). Here, the eight additional amide residues that are missing cross peaks in reduced *Ec*-Trx, Cys35–Glu39 and Ser73–Ile75, are at the N-terminal end of a helix containing the active site and a loop near this site, respectively. Note that in *S. cerevisiae* Trx2 the residues equivalent to *Ec*-Trx residues Ser73–Ile75 were reported to be considerably

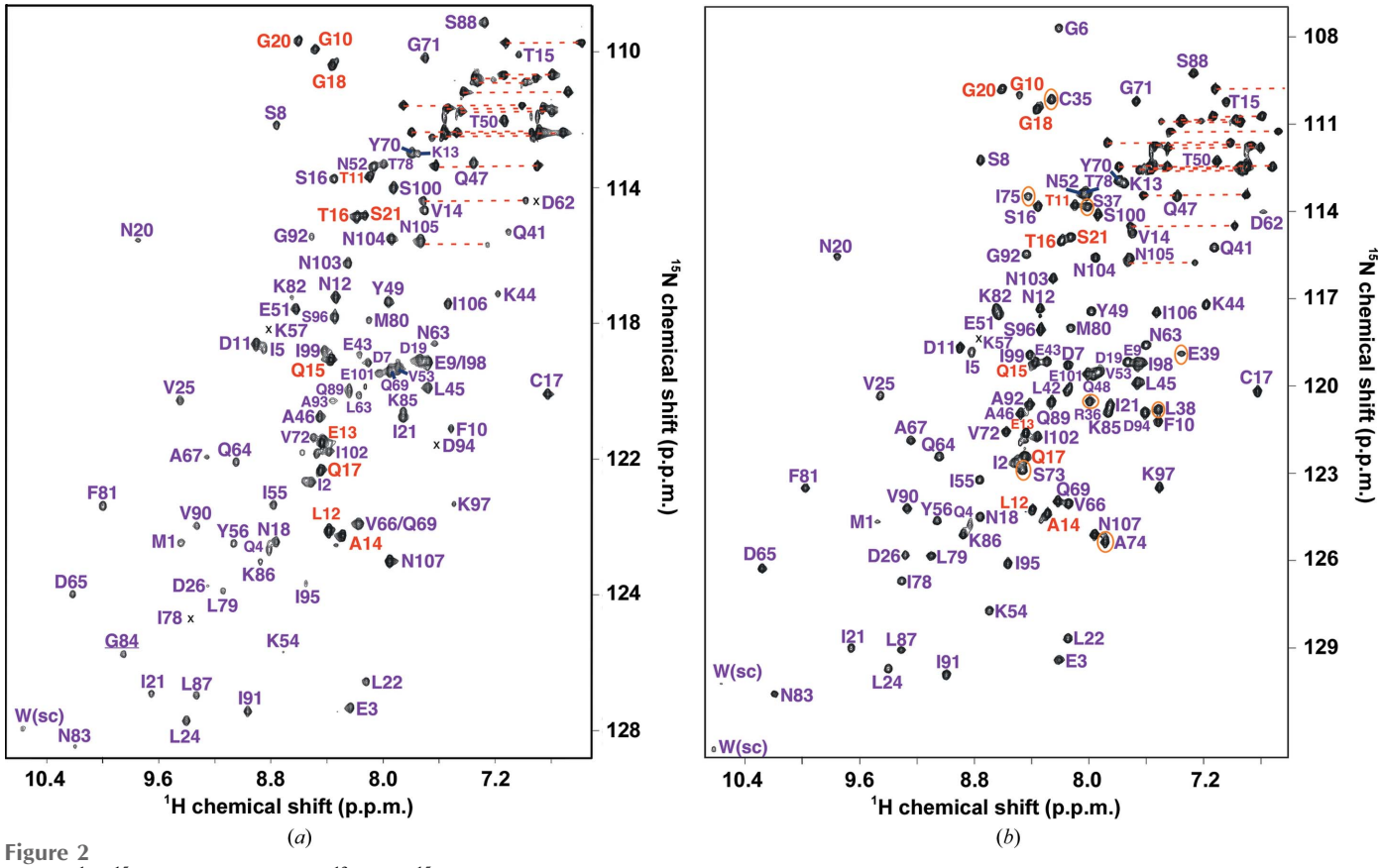

Figure 2
(*a*) The ^{1}H–^{15}N HSQC spectrum of ^{13}C- and ^{15}N-labeled reduced *Ec*-Trx (~1.0 m*M*) collected at a proton resonance frequency of 750 MHz at 20°C in 100 m*M* NaCl, 20 m*M* Tris, 1 m*M* DTT pH 7.0, with the assigned amide cross peaks labeled. Gly84 (underlined) is folded into the spectrum and Gly6, at 9.20 (^{1}H) and 107.4 (^{15}N) p.p.m., is not shown. (*b*) The ^{1}H–^{15}N HSQC spectrum of ^{13}C- and ^{15}N-labeled oxidized *Ec*-Trx (~1.0 m*M*) collected at a proton resonance frequency of 600 MHz at 20°C in 100 m*M* NaCl, 20 m*M* Tris pH 7.0, with the assigned amide cross peaks labeled. Not shown is the cross peak for Gly84 at 9.85 (^{1}H) and 103.9 (^{15}N) p.p.m. In both spectra the backbone amide cross peaks from the non-native N-terminal tag are identified with red labels, cross peaks below the displayed contour levels are identified with an 'x', side-chain amide resonance cross-peak pairs are connected by a red dashed line and the eight amide cross peaks that are absent in Fig. 2(*a*) are circled in orange in Fig. 2(*b*).

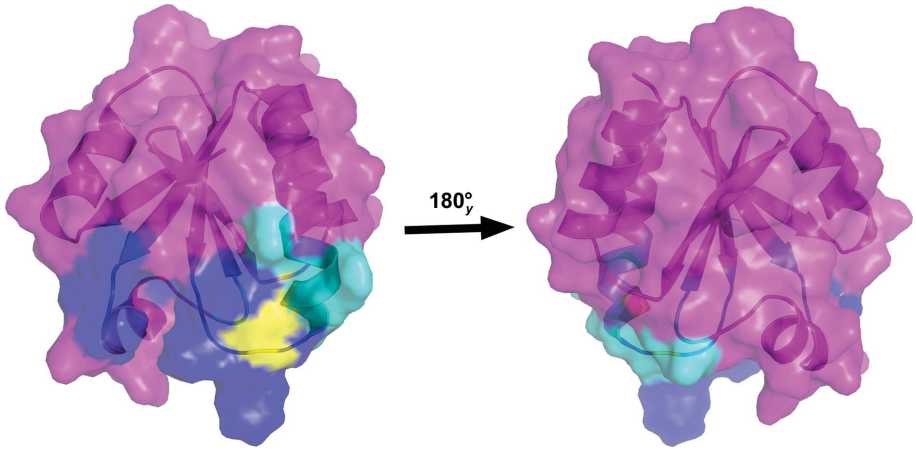

Figure 3
Both faces of the surface representation of the structure closest to the average for oxidized *Ec*-Trx, illustrating the locations of residues with missing amide cross peaks in ^{1}H–^{15}N HSQC spectra. Residues with assigned amide ^{1}H–^{15}N HSQC cross peaks are colored magenta. Residues with missing amide cross peaks in both redox states are colored blue and those missing after reduction of the Cys32–Cys35 disulfide bond are colored cyan. The active-site cysteine residues are colored yellow. The representation on the left is in approximately the same orientation as shown in Figs. 1 and 4, with the representation on the right a 180° rotation about the *y* axis.

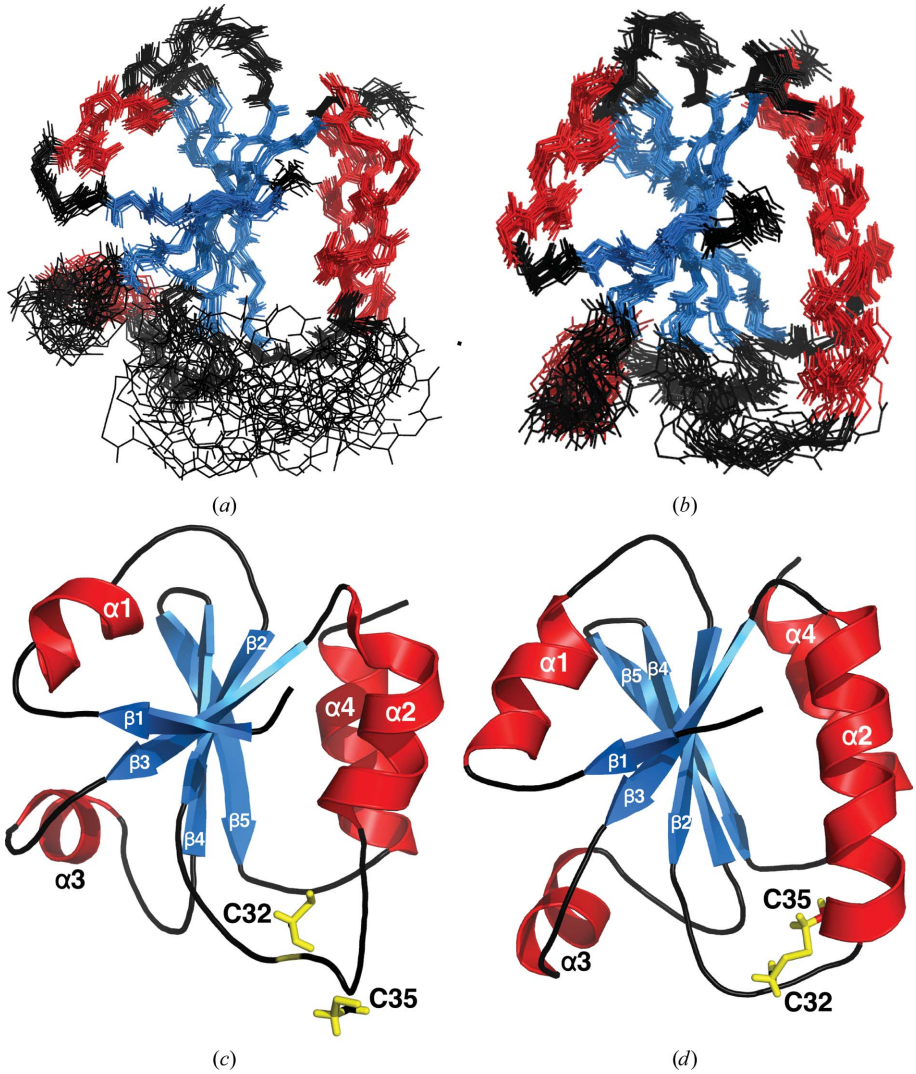

Figure 4
(*a*, *b*) Backbone superposition of the ensemble of 20 structures calculated for reduced (*a*) and oxidized (*b*) *Ec*-Trx on the structure closest to the average. (*c*, *d*) Cartoon representation of the reduced (*c*) and oxidized (*d*) *Ec*-Trx structure closest to the average structure from the ensembles in (*a*) and (*b*), respectively, to assist reference to the structure ensembles. In (*a*)–(*d*) the 21-residue N-terminal tag has been removed for clarity; the α-helices and β-strands are colored red and blue, respectively, and the side chains of the active-site cysteines are colored yellow.

line-broadened in the reduced state (Amorim *et al.*, 2007), indicating that this region in *S. cerevisiae* Trx2 was likely to be undergoing chemical exchange on a nearly similar intermediate timescale (milliseconds to microseconds). The amide resonances that are missing in both *Ec*-Trx redox states are for residues N-terminal to the residues that disappear in reduced *Ec*-Trx (Phe27–Gly33) and in a loop connecting β3 and α3 that is also near the active site (Ile58–Glu61; Fig. 1*b*). As illustrated in Fig. 3, all the missing amide resonances in both redox states (blue) or for reduced *Ec*-Trx (cyan) are clustered at or near the active site of the CGPC motif, implying intermediate timescale (milliseconds to microseconds) dynamics that expand upon breaking the Cys32–Cys35 disulfide bond.

Owing to the eight fewer amide cross peaks in the ^{1}H–^{15}N HSQC spectrum of reduced *Ec*-Trx, only 69% of the backbone and side-chain ^{1}H, ^{13}C and ^{15}N chemical shifts were assigned for reduced *Ec*-Trx, compared with the 79% assigned for oxidized *Ec*-Trx (excluding the N-terminal tag). One consequence of this assignment difference, as summarized in the structure statistics in Table 1, was 270 fewer NOEs and 12 fewer hydrogen bonds in the structure calculations for reduced *Ec*-Trx. Despite these differences in restraints, the ordered regions, as defined by the *PSVS* program, of the final ensembles of 20 structures both converged well on the average structure, with backbone (N—C$^{\alpha}$—C═O) and all-heavy-atom r.m.s.d.s of less than 0.8 and 1.2 Å, respectively. On the other hand, when using the complete native sequence (residues Met1–Asn107) for the r.m.s.d. calculations, the convergence is poorer for reduced *Ec*-Trx (1.5 and 2.1 Å) than for oxidized *Ec*-Trx (0.8 and 1.3 Å), reflecting the fewer restraints in the former calculations. The good convergence of the ordered regions of both structures is visually apparent in Figs. 4(*a*) and 4(*b*), which show a superposition of the ordered regions of the final ensemble of 20 structures upon the average structure. In both structure ensembles the region with the least convergence is also the region where the missing amides in the ^{1}H–^{15}N HSQC spectra cluster (Fig. 3): around the CGPC active site. Ensemble analysis with the *PSVS* validation software package further confirmed a quality set of final structures (Bhattacharya *et al.*, 2007). The Ramachandran statistics for the φ/ψ pairs of all of the residues in both ensembles were overwhelmingly in acceptable space (>95.8% in most favored regions and >3.1% in additionally allowed regions) and all of the structure-quality *Z*-scores were acceptable (>−2). Hence, given the available NMR data as input for the structure calculations, the final ensemble of calculated structures meets the generally accepted criteria for acceptable solution structures.

Amide cross peaks were not observed for residues Cys35–Glu39 in the reduced state of *Ec*-Trx owing to chemical exchange on the intermediate timescale (milliseconds to microseconds) that broadens these resonances beyond detection (Ådén *et al.*, 2011; Buchko *et al.*, 2016). Consequently, the difference in the length of α2 in the calculated NMR structure for reduced *Ec*-Trx is likely to be owing to the absence of NOEs and backbone hydrogen bonds to define the structure in this region of the protein and does not represent the complete unfolding of approximately half an α-helix. This conclusion is supported by the steady-state wavelength CD spectra for reduced (purple) and oxidized (red) *Ec*-Trx shown in Fig. 5(*a*). The data were obtained by first measuring the CD spectrum of oxidizing *Ec*-Trx, making the sample in the CD

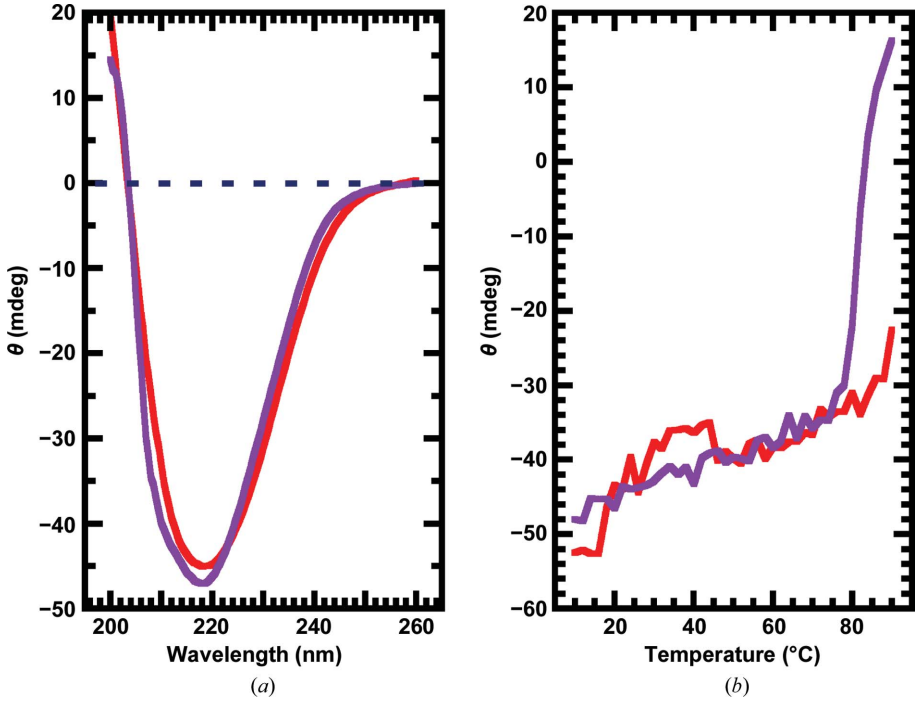

Figure 5
(*a*) Circular dichroism steady-state wavelength spectra for oxidized (red) and reduced (purple) *Ec*-Trx (~0.07 m*M*) in NMR buffer at 20°C. (*b*) The CD thermal melts for oxidized (red) and reduced (purple) *Ec*-Trx obtained by recording the ellipticity at 218 nm at 2°C intervals between 10 and 90°C.

cell 1 m*M* in DTT using a 1 *M* stock solution and collecting a spectrum for reduced *Ec*-Trx 1 h later. The spectra superimpose well and are characterized by a single minimum at ∼218 nm and an extrapolated maximum of >200 nm, which are features of a structured protein with a mixture of α-helical and β-strand components (Holzwarth & Doty, 1965). The superimposed CD profiles suggest that the structures of reduced and oxidized *Ec*-Trx are similar, and this is corroborated by similar (<1% difference) deconvolution values calculated using the *AVIV* software. More significantly, the absence of an increase in the ellipticity of the ∼218 nm CD band upon the addition of DTT to oxidized *Ec*-Trx suggests that half an α-helix does not disappear in reduced *Ec*-Trx. More likely, the full α-helix is still largely present out to Pro34, but only the backbone dynamics of the helix around the active site have changed to make it invisible in the ^{1}H–^{15}N HSQC spectrum. This illustrates that care should be taken when viewing 'disordered' regions in ensembles of NMR-based structures because the absence of canonical secondary-structure elements may be a result of the absence of NOEs owing to intermediate (millisecond to microsecond) backbone dynamics that make structure in these regions NMR-invisible.

3.4. Steady-state {^{1}H}–^{15}N heteronuclear NOEs

The missing and broadened amide resonances in the ^{1}H–^{15}N HSQC spectra of *Ec*-Trx are likely to be the result of intermediate (millisecond to microsecond) backbone dynamics in the protein backbone localized around the active site, as summarized in Fig. 3. This active site is localized on the surface of the protein to facilitate interaction with substrate (binding and reduction; Gleason & Holmgren, 1988; Collet & Messens, 2010). Localized protein dynamics are known to play a role in the binding and catalysis properties at, and around, active sites (Ishima & Torchia, 2000) and have been proposed to play a role in the activity of Trxs (Stefanková *et al.*, 2005; Amorim *et al.*, 2007). To further probe the backbone dynamics of *Ec*-Trx, this time on the fast picosecond-to-nanosecond timescale, steady-state {^{1}H}–^{15}N heteronuclear NOE ratios were collected in triplicate for *Ec*-Trx and the mean results are presented in Fig. 6. In both redox states most of the ratios are above 0.8, an approximate value typical of well structured residues. The few exceptions are the termini, where ratios below 0.8 are often observed (Peterson *et al.*, 2005), and a few isolated residues located at, or next to, loops between regions of ordered secondary structure. While these exceptions indicate localized points of thermal motion on the picosecond-to-nanosecond timescale and have been proposed to possibly play a role in switching between Trx redox states (Amorim *et al.*, 2007), the near-uniform distribution of the steady-state {^{1}H}–^{15}N heteronuclear NOE ratios above 0.8 suggest that the *Ec*-Trx structure is otherwise relatively rigid in both redox states (Peterson *et al.*, 2005).

3.5. *Ec*-Trx and conserved proline residues in the Trx scaffold

Highly conserved residues have been identified in Trxs, as illustrated for *Ec*-Trx and six other thioredoxins in Fig. 7. However, these conserved residues are all not essential for catalytic activity, but instead play roles in dictating the

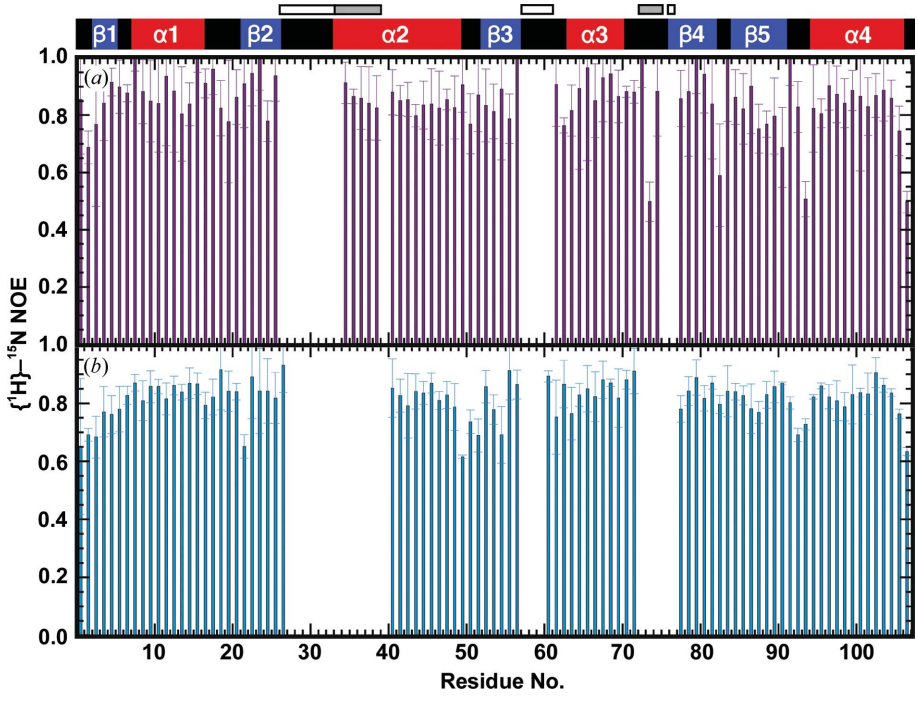

Figure 6
Backbone amide {^{1}H}–^{15}N heteronuclear NOEs for oxidized (*a*) and reduced (*b*) *Ec*-Trx collected at 20°C. On top of the plots is a schematic representation of the elements of α-helical (red) and β-strand (blue) secondary structure observed for oxidized *Ec*-Trx and the residues missing an assigned amino-acid cross peak in ^{1}H–^{15}N HSQC spectra (oxidized and reduced state colored white, reduced state only colored gray).

structure, dynamics and redox properties of the protein (Collet & Messens, 2010). Included in this group of conserved residues that are not essential for catalysis are three proline residues. In *Ec*-Trx, the first conserved proline is Pro34 located in the CGPC motif that plays a large role in determining the reducing power of Trxs (Collet & Messens, 2010). The second proline, Pro40, is six residues away from the first and serves to introduce a kink into α2 that isolates the CGPC motif from the rest of the helix (Collet & Messens, 2010), as shown here for oxidized *Ec*-Trx (Figs. 1 and 4). Proline residues in the middle of α-helices are known to introduce a kink into the helix (Woolfson & Williams, 1990). In reduced *Ec*-Trx Pro40 separates α2 into regions with amide cross peaks that are absent or present in the ^{1}H–^{15}N HSQC spectrum. As illustrated in Fig. 7, the four amino acids between the conserved last cysteine in the CGPC motif and the conserved proline appear to be semi-conserved (similar) in Trxs. However, in *Ec*-Trx only two of these four residues are semi-conserved. It may be that the SM and AE differences at the second and fourth positions, respectively, in *Ec*-Trx destabilize the N-terminus of α2 enough to introduce backbone dynamics on the millisecond-to-microsecond timescale after breaking the intramolecular Cys32–Cys35 disulfide bond. The third conserved proline residue, Pro76, is located just before β4. As described in §2.4, this proline is always observed in the *cis* conformation (Collet & Messens, 2010), and therefore, was constrained to the *cis* conformation in our structure calculations. This proline is in a loop spatially near the CGPC motif, and amide cross peaks for the three residues N-terminal to Pro76, Ser73–Ile75, are not observed in the ^{1}H–^{15}N HSQC spectrum of reduced *Ec*-Trx (Figs. 1 and 3), suggesting that the dynamics of this proximal region are also affected by the reduction of the Cys32–Cys35 disulfide bond.

3.6. Thermal stability

As described earlier, the major negative CD band for reduced and oxidized *Ec*-Trx with a minimum at ~218 nm is a spectral feature of a structured protein with a mixture of α-helical and β-strand components (Fig. 5*a*). The thermal stability of *Ec*-Trx in both redox states can be assessed by measuring the ellipticity at 218 nm at 2.0°C intervals between 10 and 90°C. In this spectral region, an increase in ellipticity with increasing temperature is generally associated with the transition from a structured to a denatured state (Karantzeni *et al.*, 2003). As shown in Fig. 5(*b*), the ellipticity for oxidized *Ec*-Trx (red) largely increases in a regular fashion from 10 to 88°C. On the other hand, the ellipticity for reduced *Ec*-Trx (purple) essentially follows the profile for oxidized *Ec*-Trx (red) until ~80°C and then increases rapidly, with precipitate observable after cooling (irreversible denaturation). This difference suggests that in the presence of an intramolecular disulfide bond the temperature of thermal denaturation increases, making the oxidized protein more stable. In general, oxidized Trxs are more stable than the reduced form, with this difference in stability being a driving force for the catalytic reaction (Collet & Messens, 2010). For example, a 12°C increase in thermal stability was observed for *E. coli* Trx between the reduced and oxidized states (Jeng *et al.*, 1994; Qin *et al.*, 1994). Because the small structural changes observed

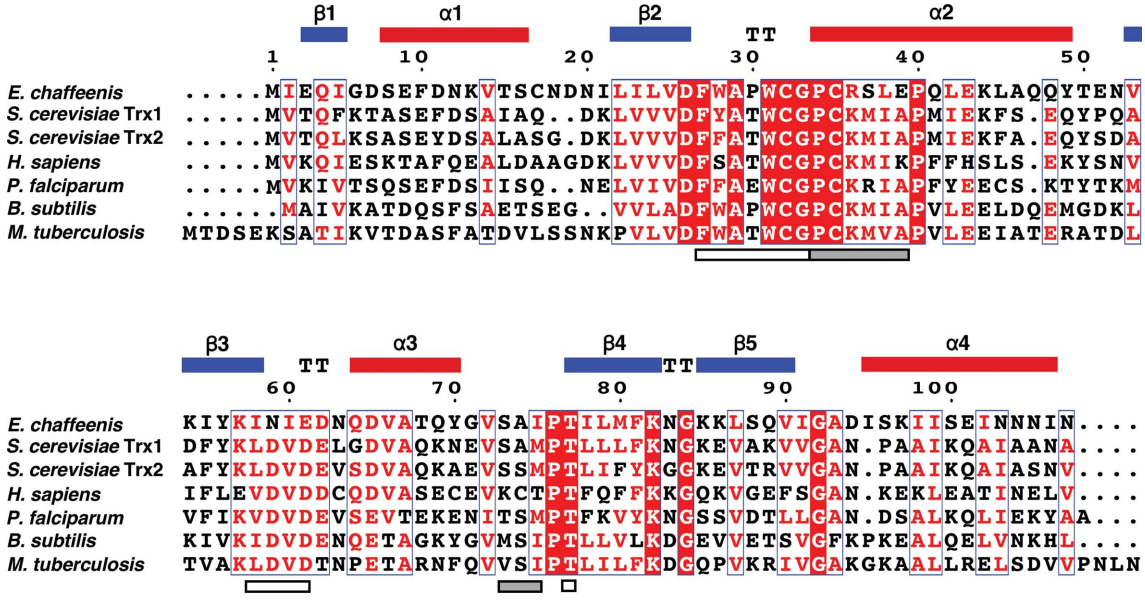

Figure 7
Clustal Omega multiple primary amino-acid sequence alignment, illustrated with *ESPript* (Robert & Gouet, 2014), of selected Trx proteins with structures in the PDB: *E. chaffeensis* (PDB entries 6amr and 6ali), *Saccharomyces cerevisiae* Trx1 (PDB entry 2i9h; Pinheiro *et al.*, 2008), *S. cerevisiae* Trx2 (PDB entry 2hsy; Amorim *et al.*, 2007), *Homo sapiens* (PDB entry 3trx; Forman-Kay *et al.*, 1991), *Plasmodium falciparum* (PDB entry 2mmn; C. Munte, H. Kalbitzer & R. Schirmer, unpublished work), *Bacillus subtilis* (PDB entry 2gzy; Li *et al.*, 2007) and *Mycobacterium tuberculosis* (PDB entry 2l59; Olson *et al.*, 2013). Above the alignment are the elements of secondary structure observed for oxidized *Ec*-Trx (α-helices colored red, β-strands colored blue). Below the alignment the residues missing an assigned amino-acid cross peak in the ^{1}H–^{15}N HSQC spectra are highlighted (oxidized and reduced state colored white, reduced state only colored gray).

between *E. coli* Trx in the reduced and oxidized states cannot account for the significant thermal and chemical stability differences between the two redox states, it was proposed that these stability differences may be owing, at least in part, to changes in the dynamic properties of *E. coli* Trx in the reduced and oxidized states (Stefanková *et al.*, 2005). The dynamic differences implied by the disappearance of eight amide cross peaks in the ^{1}H–^{15}N HSQC spectrum of reduced *Ec*-Trx (Fig. 2) may play a role in the decreased thermal stability of reduced *Ec*-Trx despite the general similarities of the structures in both redox states (Fig. 1).

4. Conclusions

The overall topology of the solution structures determined for *Ec*-Trx in the oxidized and reduced states is similar to the topology reported in other thioredoxin structures. Using the available NMR data, the length of the α-helix containing the CGPC active site (α2) was observed to extend between residues Gly33 and Tyr49 in the oxidized state but only between residues Gln40 and Gln48 in the reduced state. However, these structural differences in the catalytic helix are very likely to be owing to the absence of proton–proton NOEs that are essential to define this region during the structure calculations, making the structure NMR-invisible in this region. These NOEs are missing because eight amide cross peaks are absent in the ^{1}H–^{15}N HSQC spectrum of reduced *Ec*-Trx relative to that of oxidized *Ec*-Trx. While the absence of these cross peaks is detrimental to the structure calculations, they do identify a change in the backbone dynamics on the intermediate millisecond-to-microsecond timescale associated with the breakage of an intramolecular Cys32–Cys35 disulfide bond. Dynamics have been suggested to play a contributing role in the catalytic function of thioredoxins and their roles in the thioredoxin system. If the dynamics observed here for *Ec*-Trx are unique to the intracellular bacterium *E. chaffeenis*, this may represent a potential pathway for new intervention strategies for human monocytic ehrlichiosis.

Acknowledgements

The internal SSGCID ID for *Ec*-Trx is EhchA.00546.a. Battelle operates PNNL for the US Department of Energy.

Funding information

This research was supported by the National Institute of Allergy and Infectious Diseases (NIAID) through Federal Contract Nos. HHSN2722001200025C and HHSN272200700057C. Most of this research was performed at the W. R. Wiley Environmental Molecular Sciences Laboratory (EMSL), a national scientific user facility located on the Pacific Northwest National Laboratory (PNNL) campus and sponsored by the US Department of Energy's Office of Biological and Environmental Research Program.

References

Ådén, J., Wallgren, M., Storm, P., Weise, C. F., Christiansen, A., Schröder, W. P., Funk, C. & Wolf-Watz, M. (2011). *Biochim. Biophys. Acta*, **1814**, 1880–1890.
Amorim, G. C., Pinheiro, A. S., Netto, L. E. S., Valente, A. P. & Almeida, F. C. L. (2007). *J. Biomol. NMR*, **38**, 99–104.
Bhattacharya, A., Tejero, R. & Montelione, G. (2007). *Proteins*, **66**, 778–795.
Buchko, G. W., Clifton, M. C., Wallace, E. G., Atkins, K. A. & Myler, P. J. (2017). *Biomol. NMR Assign.* **11**, 51–56.
Buchko, G. W., Daughdrill, G. W., de Lorimier, R., Rao, B. K., Isern, N. G., Lingbeck, J. M., Taylor, J. S., Wold, M. S., Gochin, M., Spicer, L. D., Lowry, D. F. & Kennedy, M. A. (1999). *Biochemistry*, **38**, 15116–15128.
Buchko, G. W., Hewitt, S. N., Van Voorhis, W. C. & Myler, P. J. (2013). *J. Biomol. NMR*, **57**, 369–374.
Buchko, G. W., Lin, G., Tarasevich, B. J. & Shaw, W. J. (2013). *Arch. Biochem. Biophys.* **537**, 217–224.
Buchko, G. W., Perkins, A., Parsonage, D., Poole, L. B. & Karplus, P. A. (2016). *Biomol. NMR Assign.* **10**, 57–61.
Buchko, G. W., Yee, A., Semesi, A., Myler, P. J., Arrowsmith, C. H. & Hui, R. (2015). *Acta Cryst.* F**71**, 514–521.
Chen, V. B., Arendall, W. B., Headd, J. J., Keedy, D. A., Immormino, R. M., Kapral, G. J., Murray, L. W., Richardson, J. S. & Richardson, D. C. (2010). *Acta Cryst.* D**66**, 12–21.
Choi, R., Kelley, A., Leibly, D., Nakazawa Hewitt, S., Napuli, A. & Van Voorhis, W. (2011). *Acta Cryst.* F**67**, 998–1005.
Collet, J. F. & Messens, J. (2010). *Antioxid. Redox Signal.* **13**, 1205–1216.
Eklund, H., Gleason, F. K. & Holmgren, A. (1991). *Proteins*, **11**, 13–28.
Ewing, S. A., Dawson, J. E., Kocan, A. A., Barker, R. W., Warner, C. K., Panciera, R. J., Fox, J. C., Kocan, K. M. & Blouin, E. F. (1995). *J. Med. Entomol.* **32**, 368–374.
Farrow, N. A., Muhandiram, R., Singer, A. U., Pascal, S. M., Kay, C. M., Gish, G., Shoelson, S. E., Pawson, T., Forman-Kay, J. D. & Kay, L. E. (1994). *Biochemistry*, **33**, 5984–6003.
Forman-Kay, J. D., Clore, G. M., Wingfield, P. T. & Gronenborn, A. M. (1991). *Biochemistry*, **30**, 2685–2698.
Gleason, F. K. & Holmgren, A. (1988). *FEMS Microbiol. Rev.* **4**, 271–297.
Holmgren, A. (1985). *Annu. Rev. Biochem.* **54**, 237–271.
Holmgren, A. (1995). *Structure*, **3**, 239–243.
Holzwarth, G. M. & Doty, P. (1965). *J. Am. Chem. Soc.* **87**, 218–228.
Ishima, R. & Torchia, D. A. (2000). *Nature Struct. Biol.* **7**, 740–743.
Jeng, M. F., Campbell, A. P., Begley, T., Holmgren, A., Case, D. A., Wright, P. E. & Dyson, H. J. (1994). *Structure*, **2**, 853–868.
Karantzeni, I., Ruiz, C., Liu, C.-C. & Licata, V. J. (2003). *Biochem. J.* **374**, 785–792.
Laurent, T. C., Moore, E. C. & Reichard, P. (1964). *J. Biol. Chem.* **239**, 3436–3444.
Li, Y., Hu, Y., Zhang, X., Xu, H., Lescop, E., Xia, B. & Jin, C. (2007). *J. Biol. Chem.* **282**, 11078–11083.
Lu, J. & Holmgren, A. (2014). *Antioxid. Redox Signal.* **21**, 457–470.
Maiti, R., Van Domselaar, G. H., Zhang, H. & Wishart, D. S. (2004). *Nucleic Acids Res.* **32**, W590–W594.
Mustacich, D. & Powis, G. (2000). *Biochem. J.* **346**, 1–8.
Olano, J. P. & Walker, D. H. (2002). *Med. Clin. North Am.* **86**, 375–392.
Olson, A. L., Neumann, T. S., Cai, S. & Sem, D. S. (2013). *Proteins*, **81**, 675–689.
Paddock, C. D. & Childs, J. E. (2003). *Clin. Microbiol. Rev.* **16**, 37–64.
Peterson, F. C., Lytle, B. L., Sampath, S., Vinarov, D., Tyler, E., Shahan, M., Markley, J. L. & Volkman, B. F. (2005). *Protein Sci.* **14**, 2195–2200.
Pinheiro, A. S., Amorim, G. C., Netto, L. E., Almeida, F. C. & Valente, A. P. (2008). *Proteins*, **70**, 584–587.

Powis, G., Mustacich, D. & Coon, A. (2000). *Free Radic. Biol. Med.* **29**, 312–322.
Qin, J., Clore, G. M. & Gronenborn, A. M. (1994). *Structure*, **2**, 503–522.
Ravi, D., Muniyappa, H. & Das, K. C. (2005). *J. Biol. Chem.* **280**, 40084–40096.
Rikihisa, Y. (2010). *Nature Rev. Microbiol.* **8**, 328–339.
Robert, X. & Gouet, P. (2014). *Nucleic Acids Res.* **42**, W320–W324.
Sagaram, U. S., El-Mounadi, K., Buchko, G. W., Berg, H. R., Kaur, J., Pandurangi, R. S., Smith, T. J. & Shah, D. M. (2013). *PLoS One*, **8**, e82485.
Sharma, D. & Rajarathnam, K. (2000). *J. Biomol. NMR*, **18**, 165–171.
Staker, B. L., Buchko, G. W. & Myler, P. J. (2015). *Curr. Opin. Microbiol.* **27**, 133–138.
Stefanková, P., Kollárová, M. & Barák, I. (2005). *Gen. Physiol. Biophys.* **24**, 3–11.
Woolfson, D. N. & Williams, D. H. (1990). *FEBS Lett.* **277**, 185–188.
Yee, A. *et al.* (2002). *Proc. Natl Acad. Sci. USA*, **99**, 1825–1830.